Improved Electrocatalytic Activity of Size-Controlled Single-Crystalline Tungsten Oxide Nanoplates under Visible-Light Illumination

Je-Suk Moon, Young-Woo Lee, Sang-Beom Han, Choon-Koo Zhoh[*] and Kyung-Won Park[*]

Department of Chemical Engineering, Soongsil University, Seoul 156-743, Republic of Korea
[*]E-mail: ckzhoh@ssu.ac.kr; kwpark@ssu.ac.kr

We report size-controlled single crystalline $WO_3 \cdot H_2O$ nanoplates for improved electrocatalytic reaction under visible-light. The size-controlled single crystalline $WO_3 \cdot H_2O$ nanoplates were synthesized by means of hydrothermal reaction process as a function of reaction time and characterized by scanning electron microscopy, transmission electron microscopy, and X-ray powder diffraction method. The nanoplates showed a remarkably enhanced performance for methanol oxidation under AM 1.5 solar illumination as compared to that without the solar illumination. The improved photocatalytic activity of $WO_3 \cdot H_2O$ nanoplates might be related to an enhanced methanol oxidation by photo-generated holes in the $WO_3 \cdot H_2O$ under the solar illumination.

Keywords: nanostructures; oxides; chemical synthesis; visible-light; electrochemical properties

1. INTRODUCTION

Tungsten oxide materials have been utilized in a variety of fields, such as electrochromic devices [1-4], fuel cells [5-8], lithium ion batteries [9,10], photo-catalysis [11-15], gas sensors [16,17], heterogeneous catalysts [18,19], and solar energy devices [20,21]. In particular, WO_3 is an n-type metal oxide semiconductor with an indirect band gap of 2.6-2.7 eV, i.e. responsive to the blue end of the visible spectrum [22]. Furthermore, under the visible light excitation of the WO_3 electrode, an electron-hole pair is produced as follows:

$$WO_3 + h\nu \rightarrow WO_3 + e^- + h^+ \quad (1)$$

The photo-generated holes can react with methoxy species of methanol and oxidize as the following equations:

$$CH_3O^- + h^+ \rightarrow CH_3O^\bullet \quad (2)$$
$$CH_3O^\bullet \rightarrow CH_2O^{\bullet-} + H^+ \quad (3)$$
$$CH_2O^{\bullet-} \rightarrow CH_2O^\bullet + e^- \quad (4)$$
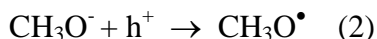
Finally, when the visible light is absorbed by WO_3, methanol is oxidized by the holes and the electrons are collected generating oxidation current as follows:

$$WO_3(h\nu) + CH_3OH + H_2O \rightarrow WO_3 + CO_2 + 6H^+ + 6e^- \quad (5)$$
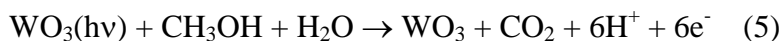
The tungsten oxide nanoparticles [23-25], nanowires [26,27], and nanoplates [28,29] have been prepared by a variety of synthetic methods [30-32]. Hydrous $WO_3 \cdot H_2O$ crystals form layers built up by corner sharing $[WO_6]$ octahedral with water molecules between these planes. Intercalated water molecules lead to $WO_3 \cdot H_2O$ layers with a basal spacing d=5.36 in orthorhombic crystal system, exhibiting enhanced intercalation properties towards cationic species, comparing with anhydrous WO_3 [33]. Especially, two-dimensional tungsten oxide nanostructures as electrochemical materials have been intensively because of active sites for photo-electrochemistry and building blocks for complex nanostructures. It has been reported that tungsten oxide nanoplates have been synthesized using a topochemical conversion reaction or anodizing process [34]. Also, it was reported that size quantization effects in the ultrathin nanostructure might alter the WO_3 band gap, representing enhanced performance for photocatalytic reduction of CO_2 in the presence of water in hydrocarbon fuels that do not exist in its bulk form [35].

Herein, we prepared single crystalline $WO_3 \cdot H_2O$ nanoplates by hydrothermal reaction process as a function of reaction time and described an improved electrocatalytic reaction for methanol oxidation of the nanoplates under AM 1.5 solar illumination. The structural and catalytic properties were characterized by means of scanning electron microscopy (SEM), transmission electron microscopy (TEM), X-ray diffraction (XRD), and voltammetry.

2. EXPERIMENTAL

To prepare $WO_3 \cdot H_2O$ nanoplates, sodium metatungstate hydrate (2 g, Aldrich) as a precursor was introduced into 140 mL of 5 M hydrochloric acid solution (Samchun, 35%) with continuous stirring at 25 ^{o}C for 1 h, and then kept at 140 ^{o}C for different reaction times (20, 40, 60, 90 and 120 min). The resulting precipitates in the solutions were cooled down to 25 ^{o}C and washed with ethanol and distilled water. The yellow powders were obtained after dying in 50 ^{o}C oven.

The morphologies of the as-synthesized $WO_3 \cdot H_2O$ nanoplates were characterized by field-emission scanning electron microscopy (FESEM, JSM-6700F), using an accelerating voltage of 15 kV and beam current of ~10 μA. The transmission electron microscopy (TEM) images were obtained on a

Tecnai G2 F30 system microscope, using an accelerating voltage of 300 kV. TEM samples were prepared by placing drops of powder suspension dispersed in ethanol on a carbon-coated copper grid. The phase and structure of the product were identified by X-ray powder diffraction (D2 PHASE SYSTEM, BRUKER), using Cu K_α source ($\lambda = 0.15406$ nm) radiation at 30 kV and 10 mA in a 2θ range from 20° to 80°.

To evaluate the electrochemical performance of the electrodes, the electrochemical curves were examined using a conventional three-electrode electrochemical system consisting of a deposited electrode, a Pt gauze, and Ag/AgCl as the working, counter, and reference electrode, respectively, at 25 °C. The tungsten oxide powder was mixed together in a bowl for a few minutes with 5 wt% Nafion solution (Aldrich), de-ionized water, and 2-propanol solution (C_3H_8O, Sigma). The paste was deposited on Indium-doped tin oxide coated transparent glasses using doctor blade technique. The film as a wording electrode was heated at 60 °C for 2 h in air atmosphere. The solution of 0.5 M H_2SO_4 or 2.0 M CH_3OH + 0.5 M H_2SO_4 was stirred constantly and purged with argon gas. The current-voltage curves were measured using a 500 W xenon lamp (XIL model 05A50KS source units) that was simulated AM 1.5 solar irradiance with the intensity of 100 mW·cm^{-2}, which was adjusted using a NREL fabricated Si reference solar cell. The working electrodes were positioned in a three-neck flask and fitted with a fused silica window faced the light source.

3. RESULTS AND DISCUSSION

Fig. 1 shows FE-SEM and FE-TEM images of $WO_3 \cdot H_2O$ particles synthesized during different reaction times from 20 to 120 min (Nano-20, Nano-40, Nano-60, Nano-90, and Nano-120). As indicated in Fig. 1(a)-(c), as the reaction times of 20 to 60 min increase, the $WO_3 \cdot H_2O$ nanoparticles exhibit side-direction growth forming nanoplates. In contrast, the Nano-90 and Nano-120 display thick nanoplates (Fig. 1(d),(e)). Form FE-TEM images (Fig. 1(f)-(j)), it is also observed that as-synthesized $WO_3 \cdot H_2O$ particles show well-edged plates with increasing reaction time by corner sharing [WO_6] octahedral with water molecules between these planes. Furthermore, high-resolution TEM (HR-TEM) images and FFT patterns indicate single-crystalline $WO_3 \cdot H_2O$ plate (Fig. 1(k)-(o)).

The XRD patterns of samples synthesized as a function of reaction time are shown in Fig. 2. All the diffraction patterns exhibit $WO_3 \cdot H_2O$ phase (JCPDS No. 84-0336) with an orthorhombic crystal structure. With increasing reaction time, the peak broadening is decreased and the relative intensity of the peak is increased, representing the formation of well-grown $WO_3 \cdot H_2O$ nanoplates as indicated in the inset of Fig. 2. From the Scherrer equation, the average particle sizes of the Nano-20, Nano-40, Nano-60, Nano-90, and Nano-120 are ~23.3, 24.2, 30.7, 37.9, and 38.1 nm, respectively.

To compare electrocatalytic reaction under visible-light illumination, commercial tungsten trioxide (Comm-WO$_3$) was prepared as shown in Fig. 3. The unit cell parameter for the Comm-WO$_3$ is determined to be a=7.297 Å, b=7.539 Å and c=7.688 Å in agreement with that of the bulk monoclinic WO_3 material with space group of P21/n (JCPDS No. 43-1035) (Fig. 3(a)). In the SEM and TEM image of Fig. 3(b) and (c), respectively, the Comm-WO$_3$ exhibits irregular shape with a few hundred

nm to a few μm in particle size. Furthermore, the Comm-WO_3 particle seems to be polycrystalline as confirmed by HR-TEM image and FFT pattern (Fig. 3(d)).
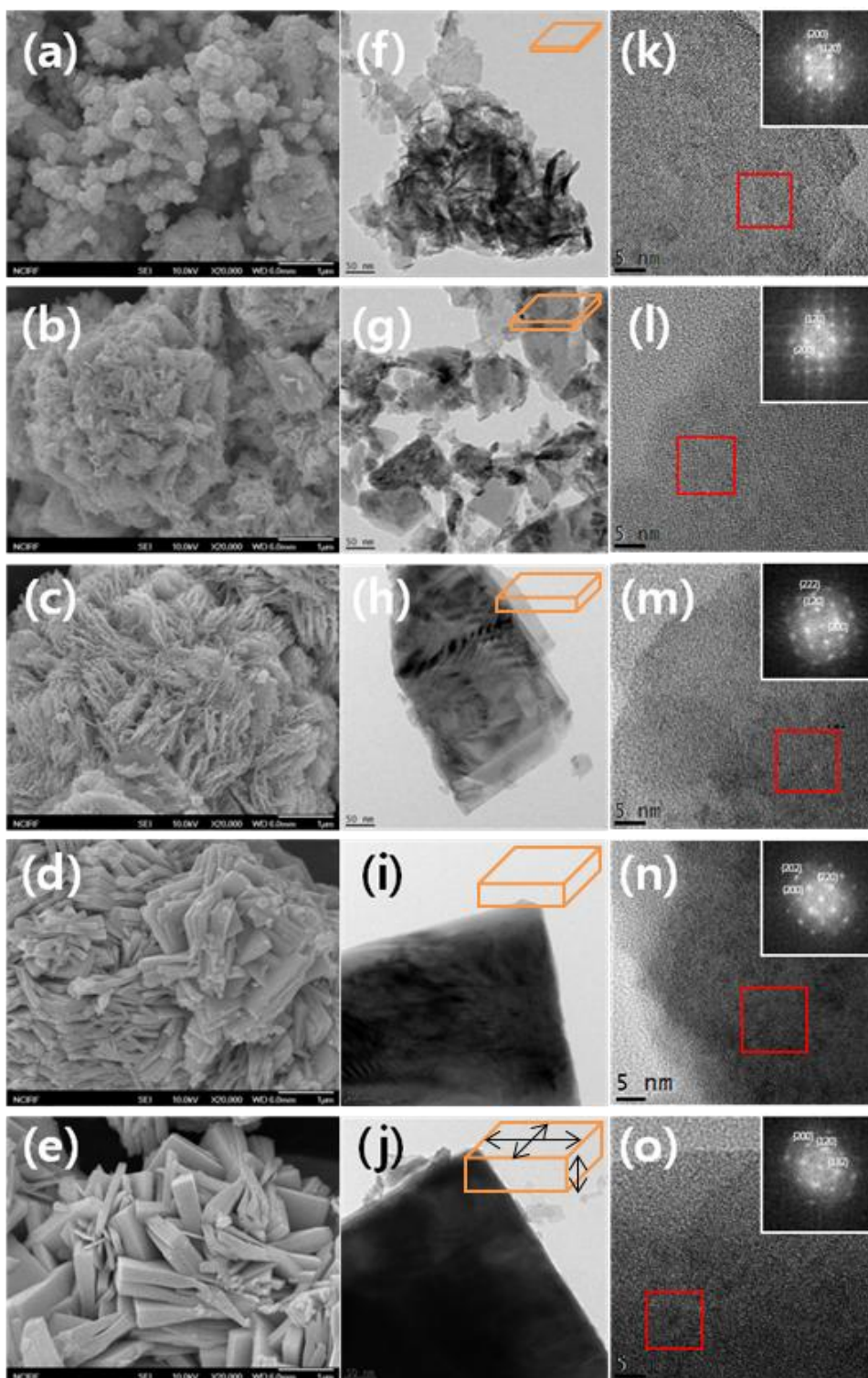
Figure 1. SEM, TEM and HR-TEM images of $WO_3 \cdot H_2O$ nanoplates synthesized during different times: (a),(f),(k) of Nano-20; (b),(g),(l) of Nano-40; (c),(h),(m) of Nano-60; (d),(i),(n) of Nano-90; (e),(j),(o) of Nano-120.
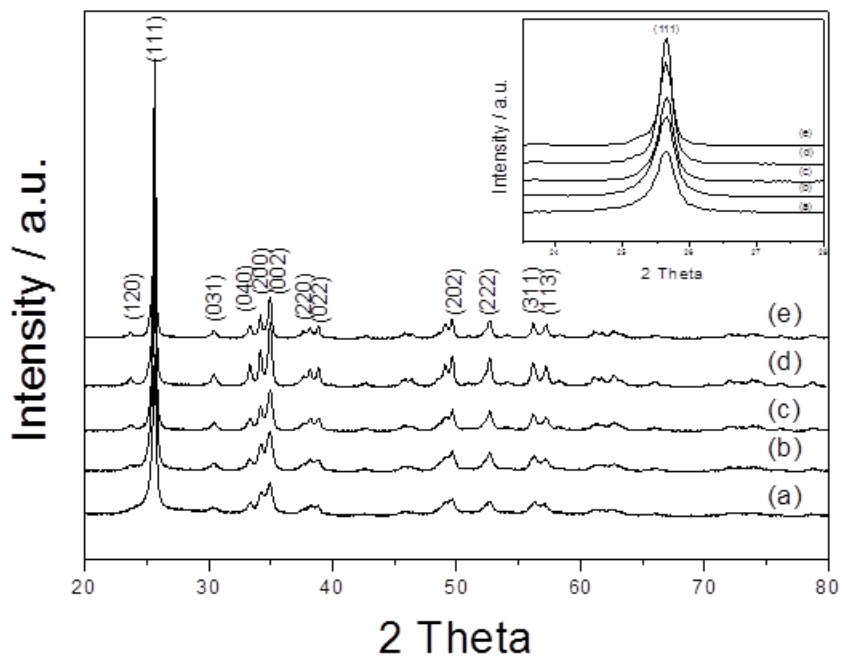
Figure 2. XRD patterns of (a) Nano-20, (b) Nano-40, (c) Nano-60, (d) Nano-90, and (e) Nano-120. The inset is the fine scan between 23.5° and 26.0°.
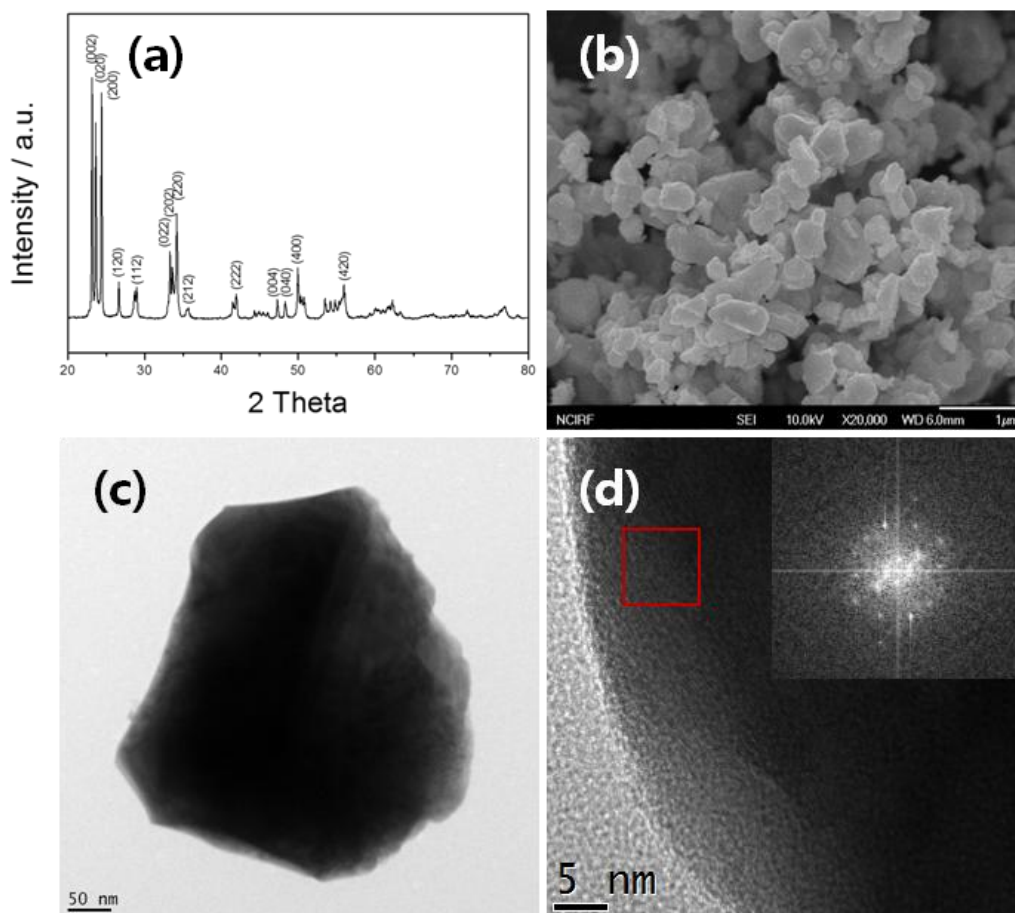
Figure 3. (a) XRD pattern, (b) SEM image, (c) TEM image, and (d) HR-TEM image of Comm-WO$_3$.
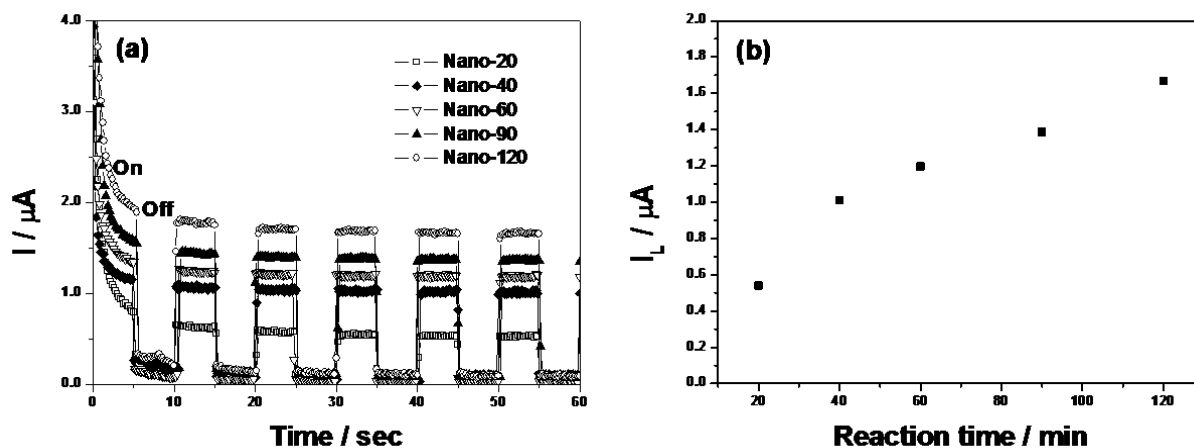
Figure 4. (a) Plots of current versus time of WO$_3$·H$_2$O nanoplates at 0.6 V by switching AM 1.5 solar illumination On/Off in 2.0 M CH$_3$OH + 0.5 M H$_2$SO$_4$. (b) Comparison of limited oxidation currents of WO$_3$·H$_2$O nanoplates under AM 1.5 solar illumination.

As shown in Fig. 4(a), plots of current versus time of WO$_3$·H$_2$O nanoplates at 0.6 V for methanol oxidation in 2.0 M CH$_3$OH + 0.5 M H$_2$SO$_4$ were detected by switching AM 1.5 solar illumination On/Off with a duration time of 5 sec. When the solar illumination source is turned on and off every 5 sec, the WO$_3$·H$_2$O nanoplates show a pulse current response every 5 sec. When the solar radiation is turned on, oxidation currents of the electrodes in 2.0 M CH$_3$OH + 0.5 M H$_2$SO$_4$ are surprisingly increased.
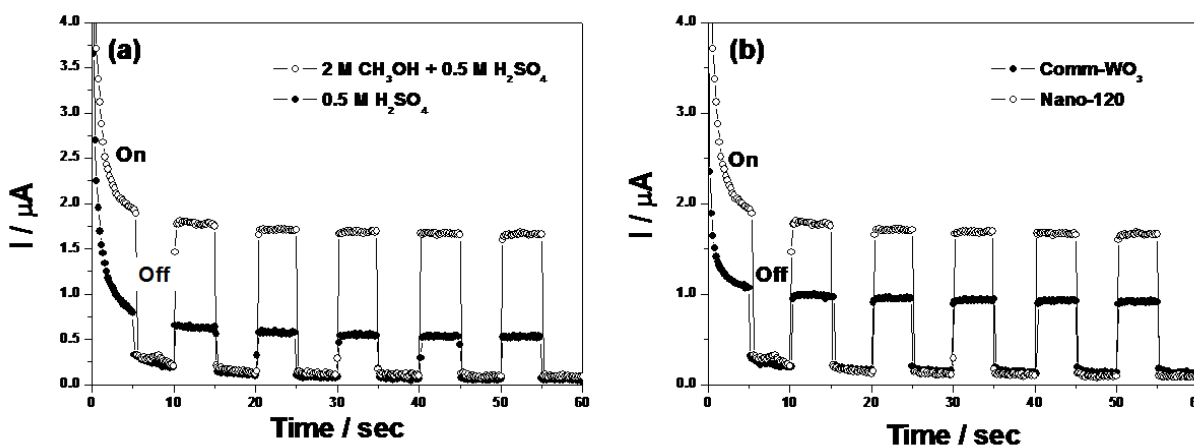
Figure 5. (a) Plots of current versus time of the Nano-120 at 0.6 V by switching AM 1.5 solar illumination On/Off in 2.0 M CH$_3$OH + 0.5 M H$_2$SO$_4$ and 0.5 M H$_2$SO$_4$. (c) Comparison of current versus time of the Nano-120 and comm-WO$_3$ at 0.6 V by switching AM 1.5 solar illumination On/Off in 2.0 M CH$_3$OH + 0.5 M H$_2$SO$_4$.

Fig. 4(b) shows limited oxidation currents under AM 1.5 solar illumination obtained from the Fig. 4(a). With increasing reaction time for synthesis of the nanoplates, the limited oxidation current increases. In particular, the Nano-120 with the most well-grown structure exhibits the highest oxidation current under the AM 1.5 solar illumination, representing much improved electrocatalytic

activity for methanol oxidation under solar radiation. On the other hand, under no radiation, i.e. dark condition, the currents of the $WO_3 \cdot H_2O$ nanoplates are reduced to almost the same level in all samples, representing no serious oxidation current without the solar radiation.

To further speculate the electrocatalytic reaction of the $WO_3 \cdot H_2O$ nanoplate with or without methanol, plots of current versus time of the Nano-120 at 0.6 V in 2.0 M CH_3OH + 0.5 M H_2SO_4 and 0.5 M H_2SO_4 were obtained as shown in Fig. 5(a). When the solar illumination source is turned on and off, the Nano-120 shows pulse current responses in 2.0 M CH_3OH + 0.5 M H_2SO_4 and 0.5 M H_2SO_4. Under no illumination, the Nano-120 represents little current in 2.0 M CH_3OH + 0.5 M H_2SO_4 and 0.5 M H_2SO_4. However, when the AM 1.5 solar illumination is turned on, the current of the electrode in 2.0 M CH_3OH + 0.5 M H_2SO_4 increases more than twice as compared to that of the electrode in 0.5 M H_2SO_4. This means that in the case of the $WO_3 \cdot H_2O$ nanoplate under the AM 1.5 solar illumination, the photocatalytic activity for methanol oxidation by photo-generated holes is more prevalent than photocurrent effect by photo-generated electron-hole pairs. Fig. 5(b) shows a comparison of current modulation of the Nano-120 with Comm-WO_3 at 0.6 V in 2.0 M CH_3OH + 0.5 M H_2SO_4. Under AM 1.5 solar radiation, the current of the Nano-120 is much higher than that of the Comm-WO_3, representing an excellent photocatalytic activity of the Nano-120. The size quantization effects in this thin-layered nanostructure of the Nano-120 might modify the energy band gap exhibiting enhanced performance for methanol oxidation by electrocatalysis under AM 1.5 solar radiation [32].

4. CONCLUSIONS

We have prepared size-controlled single crystalline $WO_3 \cdot H_2O$ nanoplates for improved electrocatalytic reaction for methanol oxidation. The as-synthesized single crystalline $WO_3 \cdot H_2O$ nanoplates showed a remarkably enhanced performance for methanol oxidation under AM 1.5 solar illumination. The well-grown Nano-120 exhibited the highest oxidation current under the AM 1.5 solar illumination, i.e. improved electrochemical performance for methanol oxidation under the solar radiation. The improved performance of the $WO_3 \cdot H_2O$ nanoplates might be due to the enhanced methanol oxidation by photo-generated holes under AM 1.5 solar illumination.

References

1. S.-H. Baeck, K.-S. Choi, T.F. Jarmillo, G.D. Stucky, E.W. McFarland, *Adv. Mater.,* 15 (2003) 126 9
2. S.-H. Lee, R. Deshpande, P.A. Parilla, K.M. Jones, B. To, A.H. Mahan, A.C. Dillon, *Adv. Mater.,* 18 (2006) 763-766.
3. Z. Jiao, X. Wang, J. Wang, L. Ke, H.V. Demir, T.W. Koh, X.W. Sun, *Chem. Commun.*, 48 (2012)

    365
4. G. A. Niklasson, C. G. Granqvist, *J. Mater. Chem.*, 17 (2007) 127
5. S. Jayaraman, T.F. Jaramillo, S.-H. Baeck, E.W. McFarland, *J. Phys. Chem. B,* 109 (2005) 2295
6. B. Wickman, M. Wesselmark, C. Lagergren, G. Lindbergh, *Electrochim. Acta,* 56 (2011) 9496
7. E. Antolini, E.R. Gonzalez, *Appl. Catal. B*, 96 (2010) 245
8. Y. Liu, S. Shrestha, W.E. Mustain, *ACS Catal.*, 2 (2012) 456
9. W.-J. Li, Z.-W. Fu, *Appl. Surf. Sci.*, 256 (2010) 2447
10. S.H. Yoom, C.S Jo, S.Y. Noh, C.W. Lee, J.H. Song, J.W. Lee, Phys. *Chem. Chem. Phys.*, 13 (2011) 11060
11. K.-W. Park, K.-S. Ahn, J.-H. Choi, Y.-C. Nah, Y.-E. Sung, *J. Phys. Chem. B*, 107 (2003) 4352
12. R. Liu, Y. Lin, L.Y. Chou, S.W. Sheehan, W. He, F. Zhang, H.J.M. Hou, D. Wang, *Angew. Chem. Int. Ed.*, 50 (2011) 499.
13. Q. Chen, J. Li, B. Zhou, M. Long, H. Chen, Y. Liu, W. Cai, W. Shangguan, *Electrochem. Commun.*, 20 (2012) 153
14. P.-T. Hsiao, L.-C. Chen, T.-L. Li, H. Teng, *J. Mater. Chem.*, 21 (2011) 19402
15. M.R. Waller, T.K. Townsend, J. Zhao, E.M. Sabio, R.L. Chamousis, N.D. Browning, F.E. Osterloh, *Chem, Mater.*, 24 (2012) 698
16. O. Berger, T. Hoffmann, W.-J. Fischer, *J. Mater. Sci. Mater. Electron*, 15 (2004) 483
17. J. Polleux, A. Gurlo, N. Barsan, U. Weimar, M. Antonietti, M. Niederberger, *Angew. Chem. Int. Ed.*, 45 (2006), 261-265.
18. M.A. Gondal, A. Hameed, Z.H. Yamani, *J. Mol. Catal. A,* 222 (2004) 259
19. H. Liu, S.J Huang, L. Zhang, S. Liu, W. Xin, L. Xu, *Catal. Commun.*, 10 (2009) 544
20. A.Z. Sadek, H. Zheng, M. Breedon, V. Bansal, S.K. Bhargava, K. Latham, J. Zhu, L. Yu, Z. Hu, P.G. Spizzirri, W. Wlodarski, K. Kalantar-zadeh, *Langmuir,* 25 (2009) 9545
21. H. Zheng, Y. Tachibana, K. Kalantar-zadeh, *Langmuir,* 26 (2010) 19148
22. Q. Mi, A. Zhanaidarova, B.S. Brunschwig, H.B. Gray N.S. Lewis, *Energy Environ. Sci.*, 5(2012) 5694
23. M, Niederberger , *Acc. Chem. Res.*, 40 (2007) 793
24. J. Polleux, N. Pinna, M. Antonietti, M. Niederberger, *J. Am. Chem. Soc.*, 127 (2005) 15595
25. N.L. Houx, G. Pourroy, F. Camerel, M. Comet, D. Spitzer, *J. Phys. Chem. C*, 114(2010) 155
26. A. Phuruangrat, D.J. Ham, S.J. Hong, S, Thongtem, J.S. Lee, *J. Mater. Chem.*, 20 (2010) 1683
27. J. Zhang, J.-P. Tu, X.-H. Xia, X.-L. Wang, C.-D. Gu, *J. Mater. Chem.*, 21 (2011) 5492.
28. K. Kalantar-zadeh, A. Vijayaraghavan, M.-H. Han, H. Zheng, M. Breedon, M.S. Strano, *Chem. Mater.*, 22 (2010) 5660
29. D. Chen, L. Gao, A. Yasumori, K. Kuroda, Y. Sugahara, *Small,* 10 (2008) 1813
30. X.-X. Zou, G.-D. LI, P.-P. Wang, J. Su, J. Zhao, L.-J. Zhou, Y.-N. Wang, J.-S. Chen, *Dalton Trans.*, 41 (2012) 9773
31. X. Su, F. Xiao, Y. LI, J. Jian, Q. Sun, J. Wang, *Mater. Lett.*, 64 (2010) 1232
32. X. He, C. Hu, Q. Yi, X. Wang, H. Hua, X. Li, *Cata. Lett.,* 142 (2012) 637
33. J. Livage, G. Guzman, *Solid State Ionics* 84 (1996) 205
34. J. Ma, J. Zhang, S. Wang, T. Wang, J. Lian, X. Duan, W. Zheng, *J. Phys. Chem. C* 115 (2011) 18157
35. X. Chen, Y. Zhou, Qi. Liu, Z. Li, J. Liu, Z. Zou, *ACS Appl. Mater. Interfaces* 4 (2012) 3372